Article

PEGylated Polyurea Bearing Hindered Urea Bond for Drug Delivery

Meishan Chen [1,2], Xiangru Feng [2,3], Weiguo Xu [2,3], Yanqiao Wang [2,3], Yanan Yang [1,*], Zhongyu Jiang [2,3,*] and Jianxun Ding [2,3]

[1] Chemical Engineering Institute, Changchun University of Technology, 2055 Yan'an Street, Changchun 130012, P. R. China; mschen@ciac.ac.cn (M.C.)
[2] Key Laboratory of Polymer Ecomaterials, Changchun Institute of Applied Chemistry, Chinese Academy of Sciences, 5625 Renmin Street, Changchun 130022, P. R. China; xrfeng@ciac.ac.cn (X.F.); wgxu@caic.ac.cn (W.X.); candyqiao77@jlu.edu.cn (Y.W.); jxding@ciac.ac.cn (J.D.)
[3] Jilin Biomedical Polymers Engineering Laboratory, 5625 Renmin Street, Changchun 130022, P. R. China
* Correspondence: zyjiang@ciac.ac.cn (Z.J.); yangyanan@ccut.edu.cn (Y.Y.)

Abstract: In recent years, polyureas with dynamic hindered urea bonds (HUBs), as a class of promising biomedical polymers, have attracted attention as a benefit of their controlled hydrolytic property. The effect of the chemical structures on the properties of polyureas and their assemblies was rarely reported. In this study, four kinds of polyureas with different chemical groups have been synthesized, and the polyurea from cyclohexyl diisocyanate and *tert*-butyl diamine showed the fastest hydrolytic rate. The amphiphilic polyurea composed of hydrophobic cyclohexyl-*tert*-butyl polyurea and hydrophilic poly(ethylene glycol) was synthesized for controlled delivery of antitumor drug paclitaxel (PTX). The PTX-loaded PEGylated polyurea micelle more effectively entered into the murine breast cancer 4T1 cells and inhibited the corresponding tumor growth *in vitro* and *in vivo*. Therefore, the PEGylated polyurea with adjustable degradation might be a promising polymer matrix for drug delivery.

Keywords: amphiphilc copolymer; hydrolyzable polyurea; micelle; controlled drug delivery; cancer chemotherapy

1. Introduction

Polyureas bearing hindered urea bonds (HUBs) are facile to be synthesized by the reaction between the monomers with diisocyanate or diamine groups [1,2]. As the orbital coplanarity of the amide bonds can be disturbed [3], HUBs are hydrolyzable, and the hydrolytic products are biologically safe [4]. Furthermore, the hydrolyzability can be regulated by changing the units of polyureas [5]. Due to the excellent hydrolyzability and biocompatibility, the polyureas have been developed for biomedical applications, such as drug delivery [6–8].

As a drug carrier, the drug release profile of polyureas can be adjusted by changing the hydrolytic rates [4], and the accumulation of therapeutic drugs at the desired tissues can also be enhanced by the passive and active targeting. For instance, Shoaib *et al*. developed several polyurethane-urea elastomers with various diisocyanate groups to deliver the antitumor drug doxorubicin (DOX). The drug release could be adjusted by changing the pH of media and hard segment chemical structures of the polyureas [9]. Morral-Ruiz *et al*. developed the biotinylated polyurethane-urea nanoparticles for target delivery of plasmid and drug [10]. The nanoparticles were loaded with a reporter gene-containing plasmid and antitumor drug for simultaneous theranostic of cancer cells. The nanoplatforms based on biotinylated polyurethane-ureas were potentially used for the therapy of other types of cancer. John *et al*. synthesized a series of polyureas with disulfide linkages in the backbone, and the antitumor drug DOX was encapsulated by the

Preprints (www.preprints.org) | NOT PEER-REVIEWED | Posted: 8 April 2019 doi:10.20944/preprints201904.0075.v1

Peer-reviewed version available at Molecules 2019, 24, 1538; doi:10.3390/molecules24081538

nanocarriers [11]. The drug-loaded nanocarriers demonstrated the glutathione-responsive drug release profile, indicating great potential for controlled drug delivery. Although the polyureas have been widely explored as the nanocarrier due to the biological safety and modifiability, the effect of the chemical structures of HUBs on the properties of hydrolysable polyureas as the drug nanocarrier was rarely reported.

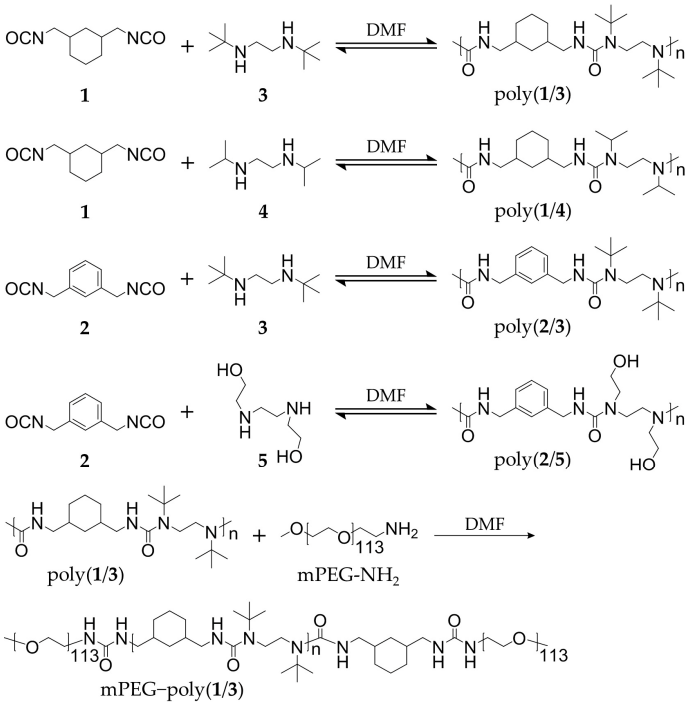

Scheme 1. Synthetic routes of hydrolyzable polyureas.

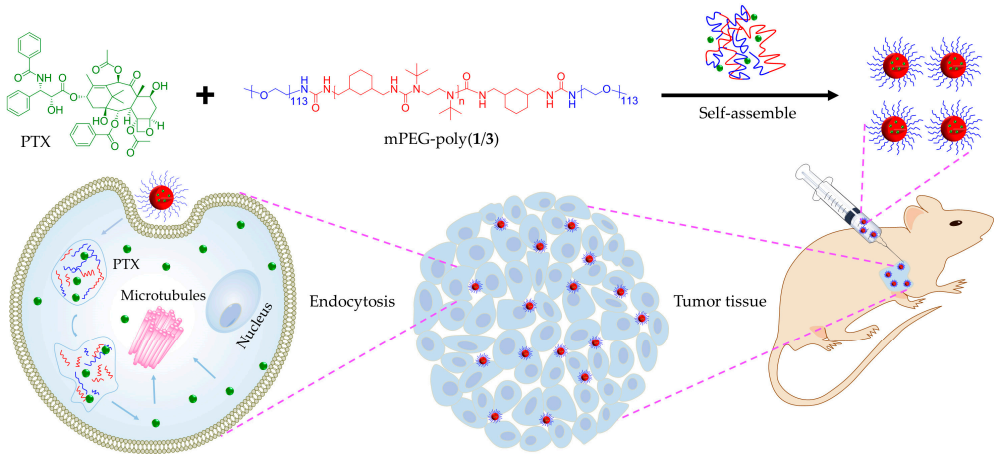

Scheme 2. Encapsulation of PTX into mPEG–poly(**1/3**) micelle to obtain PUM/PTX, and cell uptake and intracellular PTX release of PUM/PTX after intratumoral administration.

In our study, a series of hydrolyzable polyureas with different chemical structures were synthesized through different diisocyanate monomers (*i.e.*, cyclohexyl and benzyl diisocyanates) and diamine monomers (*i.e.*, isopropyl, *tert*-butyl, and hydroxyethyl diamines). The polyureas denoted as poly(**1/3**), poly(**1/4**), poly(**2/3**), and poly(**2/5**), as depicted in Scheme 1. The four polyureas showed distinct hydrolytic rates. Among the obtained polyureas, poly(**1/3**) with the fastest hydrolytic property had the most ideal potential as nanocarrier for drug release. As the amphiphilic PEGylated polyurea, mPEG–poly(**1/3**) composed of hydrophilic amino-terminated mPEG (mPEG$_{113}$-NH$_2$) and hydrophobic poly(**1/3**), was synthesized according to the reaction between amino group of mPEG and isocyanate group of polyurea. In addition, paclitaxel (PTX) as a traditional hydrophobic antitumor agent was loaded into mPEG–poly(**1/3**) to obtain the

drug-loaded polyurea micelle (PUM/PTX), as shown in Scheme 2. PUM/PTX could be efficiently internalized by mice breast tumor (4T1) cells and showed noticeable cytotoxicity *in vitro*. Moreover, PUM/PTX was also proved to be potent in inhibiting growth of the murine breast tumor compared with PTX treatment alone *in vivo*. Both histopathology and immunofluorescence were further conducted to validate the enhanced antitumor effect and biological safety of PUM/PTX. In conclusion, the PEGylated polyurea with adjustable degradation might be a meaningful polymer for drug delivery.

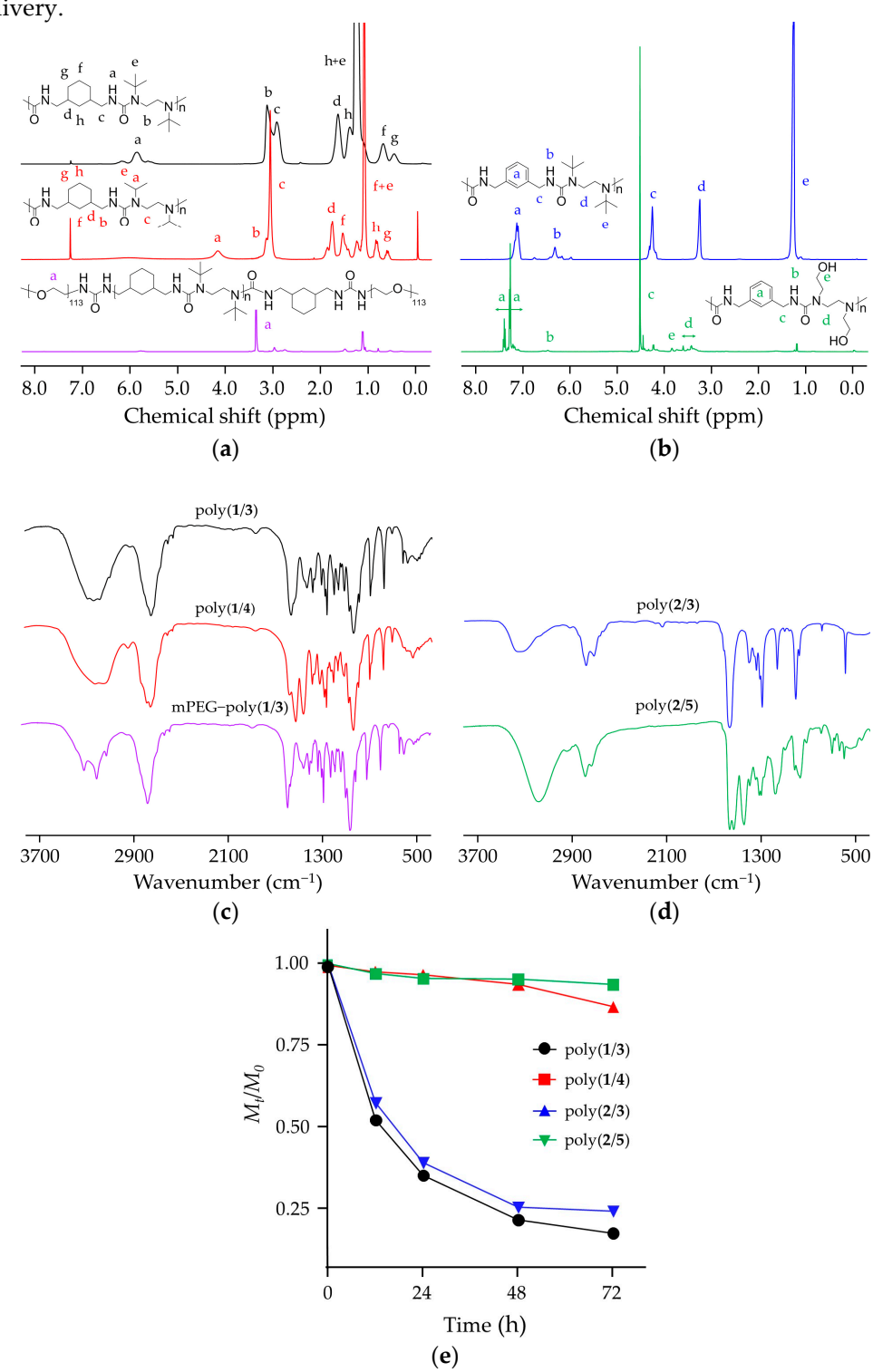

Figure 1. Characterizations of polyureas bearing HUBs. (**a**) ^{1}H NMR spectra of poly(**1**/**3**), poly(**1**/**4**), and mPEG–poly(**1**/**3**) in $CDCl_3$; (**b**) ^{1}H NMR spectra of poly(**2**/**3**) and poly(**2**/**5**) in $CDCl_3$; (**c**) FT-IR spectra of poly(**1**/**3**), poly(**1**/**4**), and mPEG–poly(**1**/**3**); (**d**) FT-IR spectra of poly(**2**/**3**) and poly(**2**/**5**); (**e**) Changes of M_ns of four polyureas with different chemical groups by GPC.

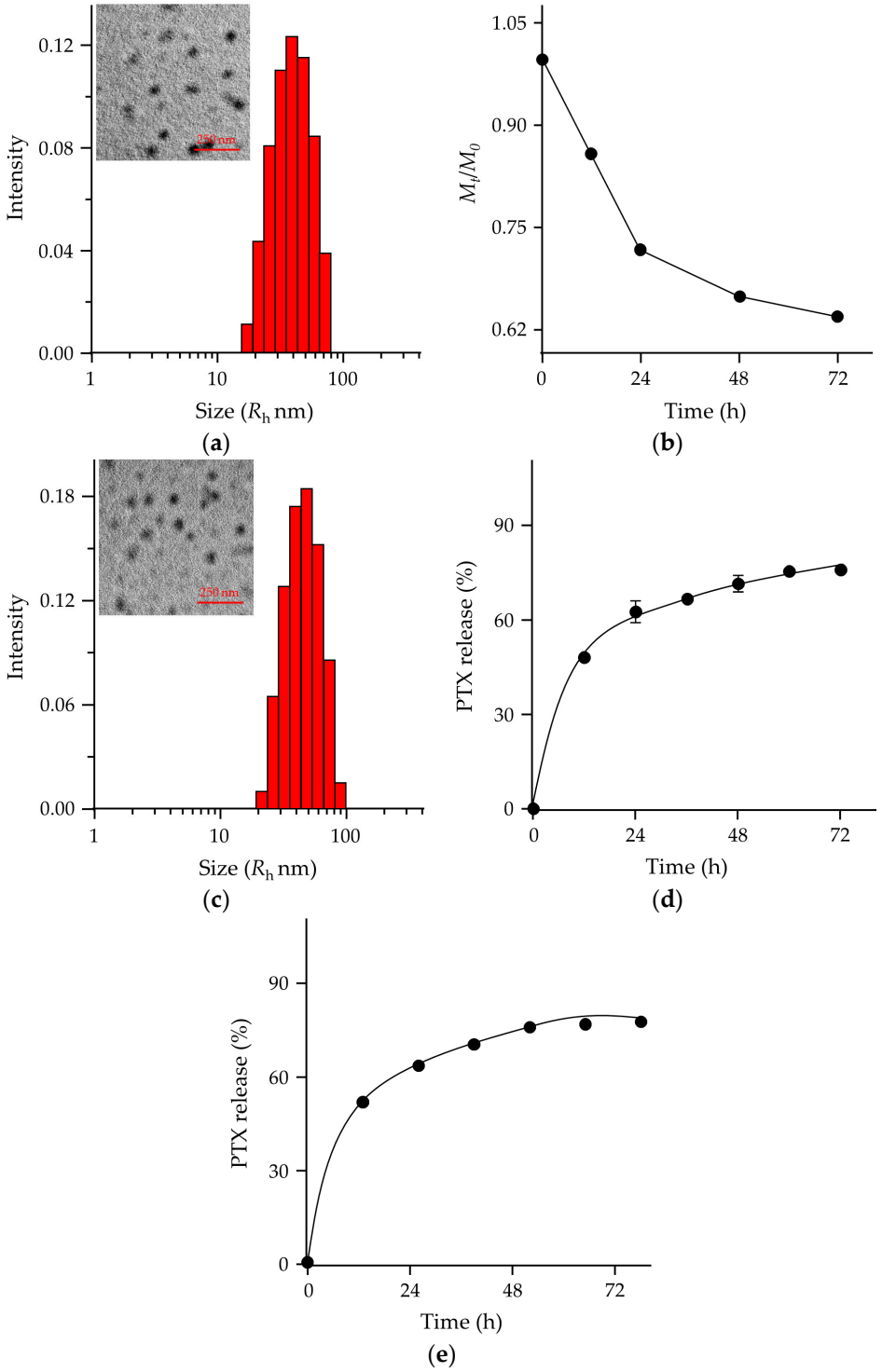

Figure 2. Characterizations of PUM and PUM/PTX. (**a**) TEM image and R_h of PUM in PBS; (**b**) M_n change of PUM by GPC; (**c**) TEM image and R_h of PUM/PTX in PBS; (**d**, **e**) PTX release behavior of PUM/PTX in PBS at pH 7.4 (**d**) and pH 6.8 (e).

2. Results and Discussion

2.1. Syntheses and Characterizations

Four kinds of hydrolyzable polyureas with different chemical groups were successfully synthesized. Briefly, equal molar (1.0 mmol) of **1** and **3**, **1** and **4**, **2** and **3**, or **2** and **5** were mixed in deuterated chloroform ($CDCl_3$, 5.0 g). The solutions were vigorously stirred at room temperature overnight, 2-fold diluted without purification and directly characterized by proton nuclear magnetic resonance (^{1}H NMR). All peaks in the ^{1}H NMR spectra of polymers were accurately assigned (Figure

1a, b). The characteristic peaks at 5.87, 6.29, and 6.46 ppm were attributed to the hydrogen atom in HUBs. The typical resonances at 1.12 − 1.30 and 3.62 − 4.70 ppm represented the substituents on a nitrogen atom. Fourier-transform infrared (FT-IR) spectroscopy further confirmed the chemical structures of polyureas as the ^{1}H NMR results. The typical signals of ureas were at 3300 − 3320 cm^{-1}. The typical wavenumbers of PEG were at 1360, 1297, and 1249 cm^{-1}. These results demonstrated that the hydrolyzable polyureas were successfully synthesized (Figure 1c, d).

The number-average molecular weights (M_ns) of polyureas were obtained from gel permeation chromatography (GPC) at the scheduled time points (Figure 1e). It was observed that the hydrolytic rates of poly(**1**/**3**) and poly(**2**/**3**) in mixed solution were faster than poly(**1**/**4**) and poly(**2**/**5**). After 48 h, M_ns reduction percentages of poly(**1**/**3**), poly(**2**/**3**), poly(**1**/**4**), and poly(**2**/**5**) were 78.4%, 74.6%, 6.4%, and 4.8%, respectively. The hydrolytic rate of poly(**1**/**3**) increased to 82.5% after incubation for 72 h. The results could be explained that the bulky substituents incorporated into one of the nitrogen atoms [12]. Urea bonds could be easily destabilized by disarranging the orbital coplanarity of the amide bonds and diminished the conjugation effect. Urea bonds with bulky substituent could dissociate into isocyanate and amines reversibly. Isocyanates could hydrolyze into amines and carbon dioxide (CO_2) in aqueous solution. It was an irreversible reaction that shifted the balance to aid the HUBs dissociation reaction and finally led to the entire hydrolysis of HUBs. Since poly(**1**/**3**) had a suitable hydrolytic time, it was selected for the following experiments.

In order to increase the hydrophilia of polyureas, mPEG was attached to both ends of poly(**1**/**3**). The ^{1}H NMR spectrum of mPEG−poly(**1**/**3**) dissolved in $CDCl_3$ indicated the successful synthesis of PEGylated polyurea (Figure 1a). In mPEG−poly(**1**/**3**), mPEG segment was hydrophilic segment, and poly(**1**/**3**) moiety was hydrophobic moiety. The amphiphilic mPEG−poly(**1**/**3**) could form into micelle in phosphate-buffered saline (PBS). Observed by transmission electron microscopy (TEM) (Figure 2a), the PUM showed a spherical structure with a mean radius of around 38 nm. The hydrodynamic radius (R_h) of PUM determined by dynamic laser light scattering (DLS) was 39.6 ± 8.1 nm. The radius of PUM examined by TEM, showed similar results with DLS. In order to explore the hydrolytic characteristics of mPEG−poly(**1**/**3**), the M_ns were detected at the scheduled time points. The PUM exhibited desired hydrolytic rates in PBS, which was similar to poly(**1**/**3**). After incubation for 48 h, the M_n of PEGylated PUM was reduced to 71.5% (Figure 2b).

The drug encapsulation capability is another important requirement for a suitable drug delivery system [13]. In order to explore the drug loading properties of polymer, PTX was loaded into mPEG−poly(**1**/**3**) micelle to form PUM/PTX. The drug loading content (DLC) and drug loading efficiency (DLE) were computed using the following equations (Eqs.) (1) and (2) [14].

$$\text{DLC} = \frac{\text{weight of drug in the PUM/PTX}}{\text{weight of drug and material}} \times 100\% \quad (1)$$

$$\text{DLE} = \frac{\text{weight of drug in the PUM/PTX}}{\text{weight of the added drug}} \times 100\% \quad (2)$$

PTX was successfully loaded into mPEG−poly(**1**/**3**) with DLC of 8.7% and DLE of 87.5%. The morphological characteristic of PUM/PTX was observed by TEM (Figure 2c), and the average particle size was around 43 nm. The R_h was 44.7 ± 11.6 nm by DLS test, showing a similar result with TEM. The results suggested that PUM/PTX was monodisperse micelle and had a uniform particle size distribution.

2.2. PTX Release, in vitro Cell Uptake, and Cell Proliferation Inhibition

The release characteristics of PTX from PUM/PTX were detected in PBS. As depicted in Figure 2d, the release profile showed no obvious burst release of PTX from PUM/PTX in PBS at pH 7.4 within 24 h. The amount of PTX released from PUM/PTX was lower than 45% during the first 12 h. At 48 h, over 65% of PTX was released. Since the tumoral microenvironment is more acidic, the PTX release behavior was also tested in PBS at pH 6.8 (Figure 2e). The amount of PTX released from PUM/PTX was 46% at the first 12 h. At 60 h, about 69% of PTX was released. These two release rates

indicated that the hydrolytic rate of PUM was faster in the acidic condition. This controlled release pattern indicated that polyurea could be used as a suitable drug delivery system.

Drug release was a complex process [15]. To simply explain the nature of drug release behaviors, a classic empirical equation was established by Peppas *et al*. [16]. The eqs. were written as:

$$\frac{M_t}{M_\infty} = k\,t^{\mathrm{n}} \tag{3}$$

$$\lg\left(\frac{M_t}{M_\infty}\right) = \lg k + \mathrm{n}\lg t \tag{4}$$

In eq (3) and (4), M_t and M_∞ were the cumulative drug release at time t and infinite time, respectively; k was the proportionality constant, and n was the release exponent that it was related to the release mechanism of payloads. In the study of drug release, the increase in n indicated that the release was more influenced by a swelling controlled way. n was calculated using the eqs. (3) and (4), and the values of pH 6.8 and 7.4 were 0.32 and 0.21, respectively. The values of n were larger at pH 6.8 than pH 7.4, which was attributed to the faster hydrolysis of polyurea in an acidic environment.

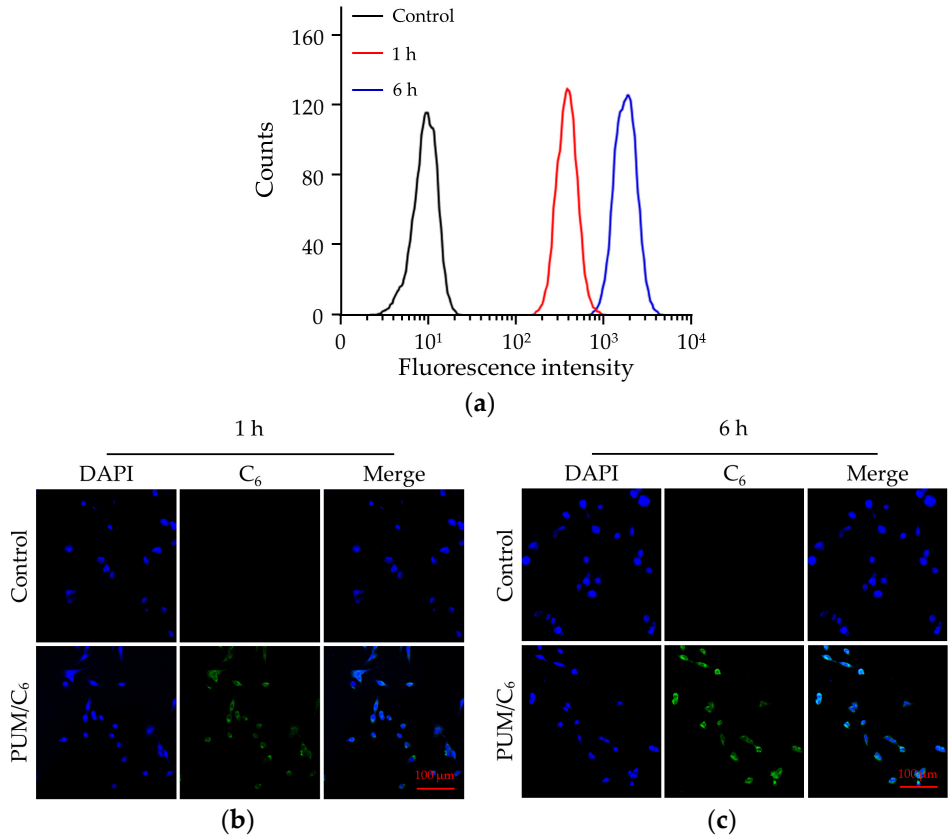

Figure 3. Cell uptake of PUM/C$_6$ after incubation with 4T1 cells detected by (**a**) FCM and (**b**, **c**) CLSM analyses in 1 h (**b**) and 6 h (**c**).

Coumarin-6 (C$_6$) as a hydrophobic model fluorescence molecule was used for cell uptake study [17]. C$_6$ was loaded into mPEG−poly(**1**/**3**) micelle to form PUM/C$_6$. The internalization of PUM/C$_6$ by 4T1 cells was monitored through flow cytometry (FCM) and confocal laser scanning microscopy (CLSM). As shown in Figure 3a, after 1h incubation, the control group had no fluorescence signals of C$_6$ while in the PUM/C$_6$ group the fluorescence signals were significantly increased, and fluorescence intensity was further increased at 6 h. Similarly, CLSM images in Figure 3b, c showed that the highest fluorescence intensity was detected when PUM/C$_6$ was incubated with 4T1 cells for 6 h. The results demonstrated that the PUM micelle could efficiently deliver PTX into 4T1 cells.

PUM with HUBs was synthesized by the reversible reaction between cyclohexyl diisocyanate and *tert*-butyl diamine. With the hydrolysis of PUM, degradation products were

Preprints (www.preprints.org) | NOT PEER-REVIEWED | Posted: 8 April 2019 doi:10.20944/preprints201904.0075.v1

Peer-reviewed version available at Molecules 2019, 24, 1538; doi:10.3390/molecules24081538

cyclohexane-1,3-diyldimethanamine and *tert*-butyl diamine. The cytotoxicity of hydrolytic products of HUBs to 4T1 and L929 cells was tested by methyl thiazolyl tetrazolium (MTT) assays (Figure 4a, b). After incubation with PUM at the concentration of 100.0 μg mL^{-1} for 72 h, the viability of L929 cells was kept around 93%, indicating negligible toxicity of PUM to normal cells. After incubation with PUM for 72 h at the concentration of 50.0 μg mL^{-1}, the cell viability of 4T1 cells was 86.97%, indicating that the polymer had little effect on the growth of tumor cells. The toxicity of free PTX and PUM/PTX toward 4T1 cells was compared by MTT assays. Both free PTX and PUM/PTX inhibited the growth of 4T1 cells. The cell viability was reduced to 51.9% after incubation with free PTX for 48 h at a concentration of 10.0 μg mL^{-1}, while cells treated with an equivalent dose of PUM/PTX showed viability of 46.6% (Figure 4c). As shown in Figure 4d, the cell proliferation was further suppressed at 72 h with cell viability reduced to around 45.9%. The data above confirmed that PUM/PTX could be efficiently endocytosed by 4T1 cells and release PTX to perform the antitumor effect. *In vitro* experiments proved that the polymer could make a proper drug delivery vehicle.

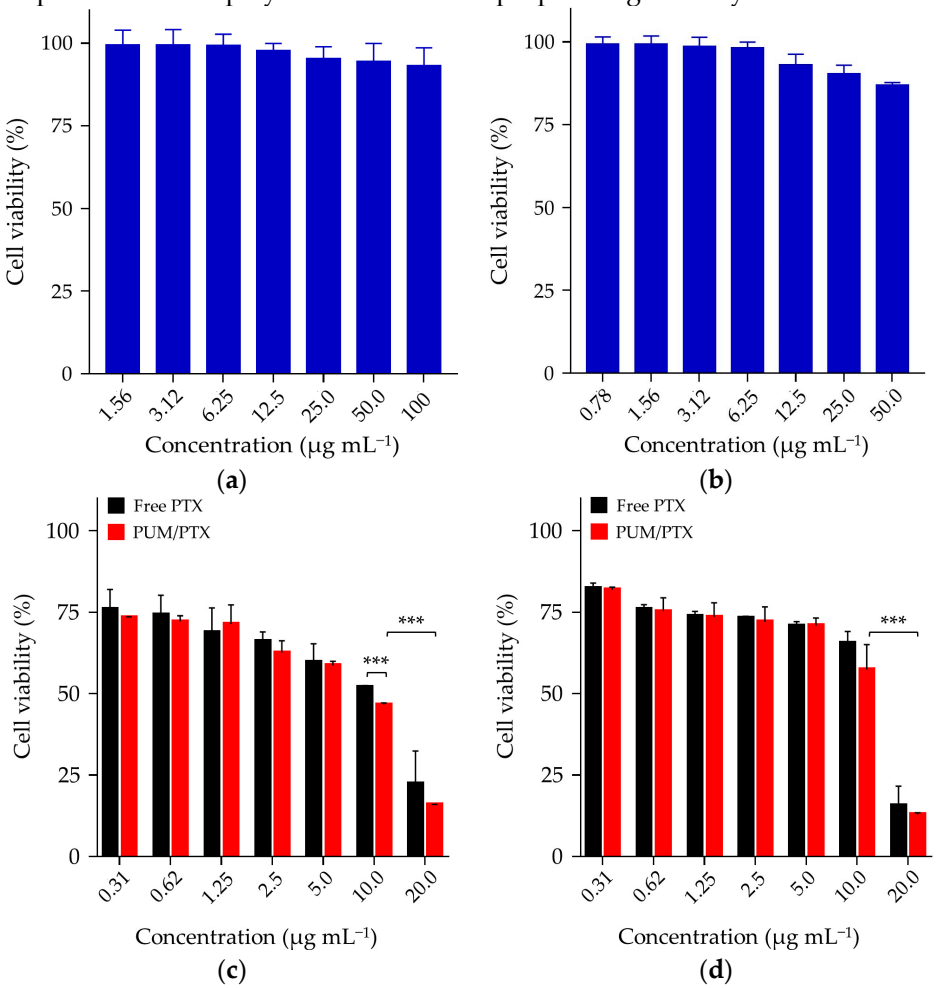

Figure 4. *In vitro* cytotoxicities of (**a**) L929, and (**b**) 4T1 cells in 72 h; (**c**) PUM/PTX in 48 h and (**d**) PUM/PTX in 72 h after incubation with 4T1 cells. The error bars represent the standard deviation (n = 3; *P < 0.05, **P < 0.01, ***P < 0.001).

2.3. In vivo Antitumor Efficacy

The antitumor activity was investigated in a BALB mice model bearing orthotopic 4T1 tumor. The antitumor efficacy of PUM/PTX was further detected *in vivo*. Free PTX was dissolved in the mixture of castor oil and ethanol [18], and diluted with PBS. The mice were treated with free PTX or PUM/PTX at a dosage of 5.0 mg kg^{-1} PTX, and the mice treated with PBS were set as a control group. The treatment started at the time when the tumor volumes reached approximately 200 mm^3. As shown in Figure 5a, free PTX showed modest antitumor efficacy compared with the control group within 18 days, whereas PUM/PTX showed the best inhibition rate of 32.7%. This result suggested

that PUM/PTX could well inhibit the tumor growth. The photograph of the tumors had a similar result (Figure 5b).

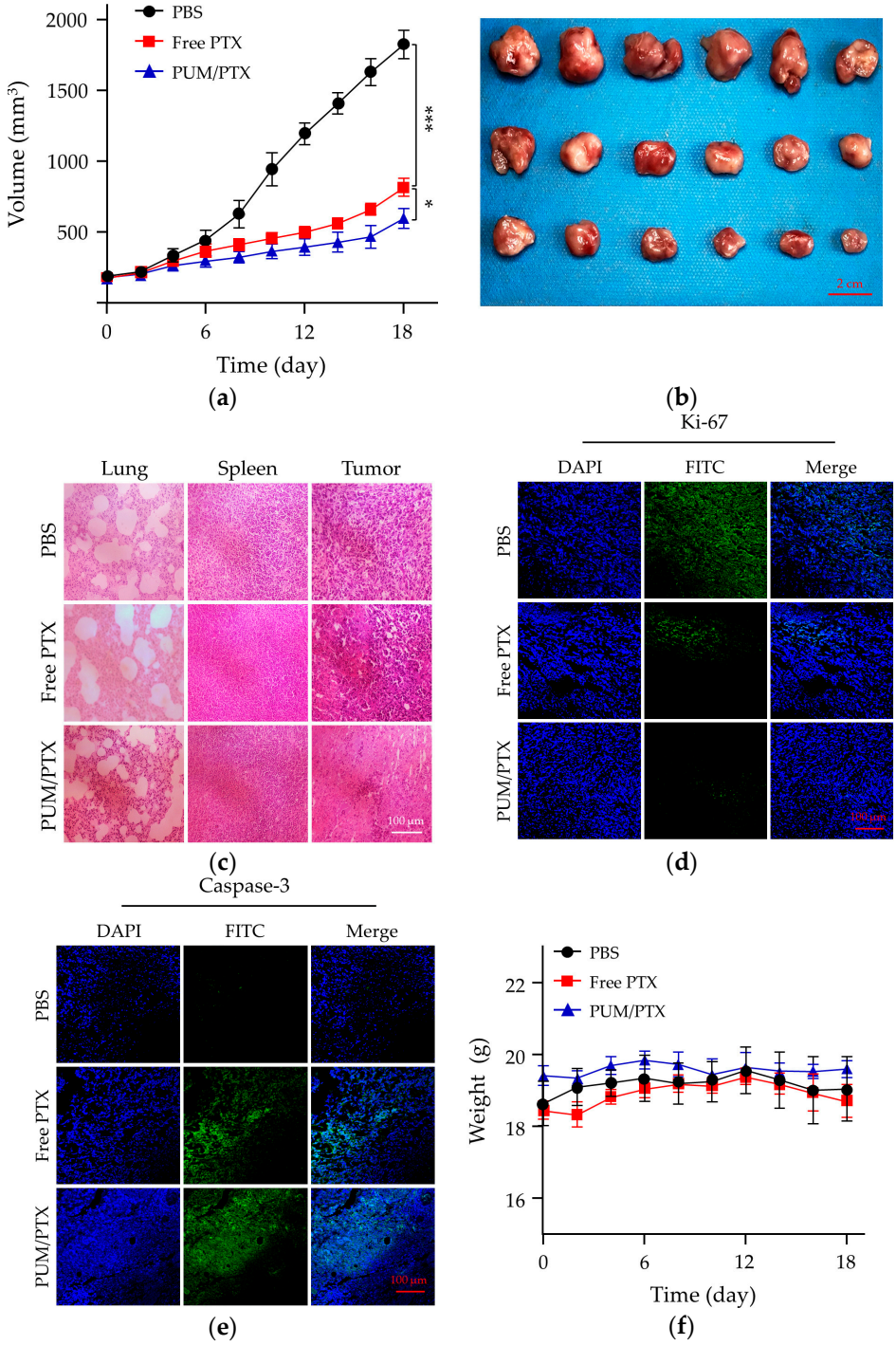

Figure 5. *In vivo* antitumor efficacy, safety assessment, and immunofluorescence experiments. (**a**) Tumor volumes, and (**b**) photograph of the isolated tumors. Data were presented as a mean ± SD (n = 6; *P < 0.05, **P < 0.01, ***P < 0.001); (**c**) H&E staining of normal organs (the lungs and spleens) and tumor tissues; (**d**) Ki-67 staining of tumor tissues; (**e**) Caspase-3 staining of tumor tissues; (**f**) the changes of body weight in each group (n = 3).

Histopathology and immunofluorescence analyses were further detected on the isolated tumors to evaluate the antitumor efficacies of PBS as control, free PTX, and PUM/PTX. In this work, lung metastasis, the trauma to healthy tissue, and the antitumor efficacies of all groups were

evaluated by hematoxylin and eosin (H&E) staining. As shown in Figure 5c, without appearance of lung metastasis, intratumoral administration of PTX and PUM/PTX at a dose of 5.0 mg kg^{-1} did not cause noticeable change in histology of the lungs and spleens. In the PTX and PUM/PTX groups, tumor cells showed volume decrease and cytoplasm denser compared with those of the control group. A large area of apoptosis appeared in the tumor tissue. The H&E results were further verified by immunofluorescence staining of Ki-67 and caspase-3. Immunofluorescence staining of Ki-67 was used to evaluate the effect of PTX formulations on the growth of tumor [19]. As shown in Figure 5d, both PUM/PTX and free PTX-treated group showed less Ki-67-positive cells. Especially, a slightly stronger antitumor effect was observed in the PUM/PTX group. The caspase-3 analysis is a common method to analyze the apoptosis of tumor cells [20]. The amount of caspase-3 suggested the apoptosis level of cells in different tumor tissues. Compared with the control group, more intense signals of caspase-3 were manifested in tumor tissues of the free PTX and PUM/PTX group, indicating larger apoptosis area (Figure 5e). These results were consistent with H&E histopathological analysis.

The body weight is an essential physiological factor to assess the toxicity of drugs [21]. As exhibited in Figure 5f, mice treated with free PTX showed an apparent decrease in body weight compared with the control group, while the body weight of mice in the PUM/PTX group remained stable. This phenomenon indicated that mPEG–poly(**1**/**3**) could efficiently improve safety. All experiments validated that mPEG–poly(**1**/**3**) could act as a suitable and biological safety drug delivery vehicle.

3. Conclusions

In this study, we synthesized four kinds of hydrolyzable polyureas with different hydrolytic rates by changing the chemical groups on the polyureas. Among them, poly(**1**/**3**) from cyclohexyl diisocyanate and *tert*-butyl diamine showed the fastest hydrolytic rate. After modification by hydrophilic mPEG, the amphiphilic mPEG–poly(**1**/**3**) was synthesized for delivery of PTX. The PTX was successfully encapsulated by mPEG–poly(**1**/**3**) micelle with DLC and DLE of 8.75% and 87.5%, respectively. PUM/PTX could be efficiently internalize by murine breast cancer 4T1 cells and release PTX along with the hydrolysis of polyurea. It showed that PUM/PTX drastically suppressed the proliferation of tumor cells *in vitro* and significantly inhibited tumor growth in an orthotopic 4T1 breast tumor model *in vivo*. Therefore, the hydrolyzable PEGylated polyureas with adjustable degradation might become a promising platform for controlled drug delivery.

4. Materials and Methods

4.1. Materials

1,3-Bis(isocyanatomethyl) cyclohexane (**1**) and 3-bis(isocyanatomethyl) benzene (**2**) were purchased from Tokyo Chemical Industry Co., Ltd. (Shanghai, P. R. China), *N,N′*-di-*tert*-butyle-thylenediamine (**3**) was purchased from Biological Science and Technology Co., Ltd. (Shanghai, P. R. China), and *N,N′*-di-*iso*-propylethylenediamine (**4**) was purchased from Aladdin (Shanghai, P. R. China), and all of them were used as obtained. *N,N′*-Bis(2-hydroxyethyl)ethylenediamine (**5**) was purchased from Energy Chemical (Shanghai, P. R. China). *N,N*-dimethylformamide (DMF) and ethyl ether were bought from Tiantai Fine Chemical Co., Ltd. (Tianjin, P. R. China). DMF was stored over calcium hydride (CaH_2) and purified by vacuum distillation. C_6 and $mPEG_{113}$-OH were purchased from Sigma-Aldrich (Shanghai, P. R. China). $mPEG_{113}$–NH_2 was prepared as our previous work [22]. PTX was purchased from Huafeng United Technology Co., Ltd. (Beijing, P. R. China). Dulbecco's modified Eagle's medium (DMEM) and newborn bovine serum (NBS) were bought from Gibco (Grand Island, NY, USA) and Every Green (Hangzhou P. R. China), respectively. Methyl thiazolyl tetrazolium (MTT) and 4′,6-diamidino-2-phenylindole dihydrochloride (DAPI) were purchased from Sigma-Aldrich (Shanghai, P. R. China). Primary antibody was purchased from Abcam Company (Cambridge, UK).

Peer-reviewed version available at *Molecules* **2019**, *24*, 1538; doi:10.3390/molecules24081538

Secondary antibody was purchased from ABclonal (Wuhan, P. R. China). The purified deionized water was prepared by the Milli-Q plus system (Millipore Co., Billerica, MA, USA).

4.2. Syntheses of Four Different Polyureas

The equimolar of **1** (1.94 g, 10.0 mmol) and **3** (1.72 g, 10.0 mmol), **1** (1.94 g, 10.0 mmol) and **4** (1.44 g, 10.0 mmol), **2** (1.88 g, 10.0 mmol) and **5** (1.48 g, 10.0 mmol), **2** (1.88 g, 10.0 mmol) and **3** (1.72 g, 10.0 mmol) were separately dissolved in anhydrous DMF (10.0 g). The solutions were vigorously stirred at room temperature overnight. 5% water was added into the polymer solutions, which were shaken at 80 rpm in 37 °C incubator. Then they were used for study of hydrolysis directly [5].

*4.3. Synthesis of mPEG–poly(**1**/**3**)*

The **1** (1.3 g, 6.7 mmol) and **3** (1.1 g, 6.5 mmol) were dissolved in anhydrous DMF, separately, and vigorously stirred at room temperature overnight. $mPEG_{113}$-NH_2 (2.5 g, 0.5 mmol) was dissolved in toluene, and residual water in the solution was removed by azeotropic distillation. The dehydrated $mPEG_{113}$-NH_2 was dissolved in anhydrous DMF, and then added into the reaction flask. The mixture was stirred at room temperature for three days, and was precipitated by anhydrous ethyl ether.

4.4. Preparation of PUM

mPEG–poly(**1**/**3**) was dissolved in dimethyl sulfoxide (DMSO) and slowly added into 0 °C PBS. The mixture solution was ultrafiltrated by ultrafiltration tube (molecular weight cut-off (MWCO) = 10,000 Da; Millipore Co., Billerica, MA, USA). Finally, the concentration of mPEG–poly(**1**/**3**) solution was kept at 1.0 mg mL^{-1}.

To investigated the hydrolysis of mPEG–poly(**1**/**3**), PUM was shaken at 80 rpm in a 37 °C incubator, 3.0 mL of the liquid was pipetted at different time points respectively, and the liquid was lyophilized. Finally, the lyophilized solids were dissolved in DMF and M_ns were monitored by GPC.

4.5. Preparation of PUM/PTX

First, mPEG–poly(**1**/**3**) and PTX were dissolved in DMSO (mass ratio of 9:1), respectively. Then two solutions were mixed evenly. The mixture was added into 0 °C PBS slowly and kept stirring quickly. Finally, the DMSO of the mixture solution was removed by ultrafiltration.

4.6. Characterizations

^1H NMR spectra were recorded on a Bruker AV 400 NMR spectrometer in $CDCl_3$. FT-IR spectra were recorded on a Bio-Rad Win-IR instrument (Cambridge, MA, USA). GPC analyses of polymers were conducted on a Waters 2414 system (Waters Co., Milford, MA, USA) equipped with Ultrahydrogel™ linear columns and a Waters 2414 refractive index detector (injection volume: 30.0 μL, column temperature: 50 °C, eluant: DMF through 0.45 μm and 0.22 μm filters, flow rate:1.0 mL min^{-1}). TEM measurements were performed on a JEOL JEM-1011 transmission electron microscope with an accelerating voltage of 100 kV. DLS measurements were performed with a vertically polarized He–Ne laser (DAWN EOS, Wyatt Technology Co., Santa Barbara, CA, USA). The high-performance liquid chromatography (HPLC) analyses of PTX were performed with a Symmetry® C18 column connected to a Waters 2487 (Waters Co., Milford, MA, USA) at a flow rate of 1.0 mL min^{-1}. DLC and DLE of PUM/PTX were determined according to the following protocol. 200.0 μL of PUM/PTX sample was mixed into 800.0 μL of acetonitrile and the detection wavelength was 227 nm.

4.7. In vitro PTX Release

PUM/PTX solution was placed into dialysis bags (MWCO = 3,500 Da). The dialysis bags were transferred into PBS (pH 6.8 and 7.4) at 37 °C with 80 rpm. The amount of released PTX was obtained by HPLC tests.

4.8. Cell Cultures

4T1 cells were cultured in complete DMEM supplemented with 10% (*V*/*V*) NBS, penicillin (50.0 IU mL^{-1}) and streptomycin (50.0 IU mL^{-1}) at 37 °C in a 5% (*V*/*V*) CO_2 atmosphere.

4.9. Cell Uptakes

PUM/C_6 was used for cell uptake study. Both CLSM and FCM investigated the cell uptake of PUM/C_6 toward 4T1 cells.

4.9.1. FCM

The cell uptake study was conducted with C_6, which was used as a hydrophobic model fluorescence probe. The cells were seeded in 6-well plates at a density of 2.0×10^5 cells each well and cultured for 12 h. Then, 100.0 μL of PUM/C_6 was added into the wells, and the cells were further incubated at 37 °C for 1 or 6 h. Next, the harvested cells were suspended in PBS and centrifuged at 1,000 rpm for 5 min. All the cells were washed with PBS. Finally, the cells were resuspended with 500.0 μL of PBS. Data were analyzed by FCM (Beckman, California, USA).

4.9.2. CLSM

The cells were seeded on the coverslips in 6-well plates with a density of 2.0×10^5 cells/well. 2.0 mL of DMEM was added into cells per well and cultured for 12 h. Then 100.0 μL of PUM/C_6 was added to each well. After incubation for 1 or 6 h, the cells were fixed with 4% (*W*/*V*) formaldehyde for 15 min. Then, the fixed cells were incubated with DAPI for 3 min and washed with PBS. The images of cell localization were observed under LSM 780 CLSM (Carl Zeiss, Jena, Germany) with 10 × eyepiece and 40 × objective.

4.10. Cytotoxicities Assays

The cytotoxicities of PUM/PTX were evaluated by the MTT assays. 4T1 cells with a density of 5×10^3 cells/well were seeded in 96-well plates in 180.0 μL of DMEM and incubated for 24 h. 20.0 μL of free PTX or PUM/PTX was added in each well with the maximum PTX concentration of 200.0 μg mL^{-1}. The cells were subjected to MTT assay after being incubated for another 48 h or 72 h. The absorbency of above solution was measured on a Bio-Rad 680 microplate reader (Hercules, CA, USA) at 490 nm. The cells viability was calculated based on the following Eq. (5).

$$\text{Cells viability (\%)} = \frac{A_{\text{sample}}}{A_{\text{control}}} \times 100\% \quad (5)$$

In Eq. (5), A_{sample} was denoted as the absorbencies of sample and A_{control} was denoted as the absorbance of the control.

The cytotoxicities of PUM to 4T1 and L929 cells were also tested at 72h. The specific steps were the same as above.

4.11. Animals Procedures

Female BALB/c mice at 5 weeks age were obtained from Vital River Laboratory Animal Technology Co., Ltd. (Beijing, P. R. China). The body weights of mice were kept between 18 − 20 g before the start of the experiment. The experiment on animals were carried out according to the guidelines outlined in the Guide for the Care and Use of Laboratory Animals, provided by Jilin University (Changchun, P. R. China) and the procedures were approved by the Animal Care and Use Committee of Jilin University.

4.12. In vivo Antitumor Efficacy

BALB/c mice were inoculated with 4T1 cells to develop the breast tumor xenograft model. 1.0×10^6 cells in 0.1 mL of PBS were injected into the right breasts. The mice were treated with PBS, PUM/PTX, or free PTX on day 0, 4, 8, 12, and 16 through intratumoral injections. The tumor volumes (V, mm^3) were estimated using the following Eq. (6) [23].

$$V\ (mm^3) = \frac{a \times b^2}{2} \quad (6)$$

In Eq. (6), a and b (mm) were the largest and the smallest axes of the tumor measured by a caliper.

4.13. Histological and Immunofluorescence Analyses

The mice were sacrificed at 2 days after the last injection. According to previous literatures, the lung is the most common organ for breast cancer metastasis, while the spleen is the major immune organ that should be observed at the end of the experiments [24]. The tumors and major organs (*i.e.*, the lungs and spleens) were collected, fixed in 4% (*W*/*V*) PBS-buffered paraformaldehyde overnight, and then embedded in paraffin. The paraffin-embedded tissues were cut into ~ 5 μm slices for H&E staining and ~ 3 μm sheets for immunofluorescence analyses (*i.e.*, Ki-67 and caspase-3). The histological and immunofluorescence alterations were detected by a microscope (Nikon Eclipse Ti, Optical Apparatus Co., Ardmore, PA, USA).

Author Contributions: J.D., W.X., and Y.Y. conceived and designed the experiments; M.C. performed the experiments; M.C., X.F., and Z.J. analyzed the data; M.C. wrote the draft manuscript; X.F., Z.J., Y.W., and J.D. revised the manuscript. All the authors confirmed the content of the manuscript and approved the submission.

Acknowledgments: This research was financially supported by the National Natural Science Foundation of China (Grant Nos. 51873207, 51803006, 51833010, 51673190, 51603204, 51673187, and 51520105004), the Science and Technology Development Program of Jilin Province (Grant No. 20190201068JC), and the National Key Research and Development Program of China (Grant No. 2016YFC1100701).

Conflicts of Interest: The authors declare no conflict of interest.

References

1. Cai, K.M.; Ying, H.Z.; Cheng, J.J. Dynamic ureas with fast and pH-independent hydrolytic kinetics. *Chem. Eur. J.* **2018**, *24*, 7345–7348.
2. Ying, H.Z.; Zhang, Y.F.; Cheng, J.J. Dynamic urea bond for the design of reversible and self-healing polymers. *Nat. Commun.* **2014**, *5*, 3218–3126.
3. Hutchby, M.; Houlden, C.E.; Ford, J.G.; Tyler, S.N.G.; Gagne, M.R.; Lloyd-Jones, G.C.; Booker-Milburn, K.I. Hindered ureas as masked isocyanates: Facile carbamoylation of nucleophiles under neutral conditions. *Angew. Chem., Int. Ed.* **2009**, *48*, 8721–8724.
4. Rocas, P.; Cusco, C.; Rocas, J.; Albericio, F. On the importance of polyurethane and polyurea nanosystems for future drug delivery. *Curr. Drug Delivery* **2018**, *15*, 37–43.
5. Ying, H.Z.; Cheng, J.J. Hydrolyzable polyureas bearing hindered urea bonds. *J. Am. Chem. Soc.* **2014**, *136*, 16974–16977.
6. Florez-Grau, G.; Rocas, P.; Cabezon, R.; Espana, C.; Panes, J.; Rocas, J.; Albericio, F.; Benitez-Ribas, D. Nanoencapsulated budesonide in self-stratified polyurethane-polyurea nanoparticles is highly effective in inducing human tolerogenic dendritic cells. *Int. J. Pharm.* **2016**, *511*, 785–793.

7. John, J.V.; Seo, E.J.; Augustine, R.; Jang, I.H.; Kim, D.K.; Kwon, Y.W.; Kim, J.H.; Kim, I. Phospholipid end-capped bioreducible polyurea micelles as a potential platform for intracellular drug delivery of doxorubicin in tumor cells. *ACS Biomater. Sci. Eng.* **2016**, *2*, 1883−1893.
8. Valerio, A.; Feuser, P.E.; Bubniak, L.D.; Dos Santos-Silva, M.C.; de Araujo, P.H.H.; Sayer, C. *In vitro* biocompatibility and macrophage uptake assays of poly(urea-urethane) nanoparticles obtained by miniemulsion polymerization. *J. Nanosci. Nanotechnol.* **2017**, *17*, 4955−4960.
9. Shoaib, M.; Bahadur, A.; Rahman, M.S.U.; Iqbal, S.; Arshad, M.I.; Tahir, M.A.; Mahmood, T. Sustained drug delivery of doxorubicin as a function of pH, releasing media, and NCO contents in polyurethane urea elastomers. *J. Drug Deliv. Sci. Tec.* **2017**, *39*, 277−282.
10. Morral-Ruiz, G.; Melgar-Lesmes, P.; Lopez-Vicente, A.; Solans, C.; Garcia-Celma, M.J. Biotinylated polyurethane-urea nanoparticles for targeted theranostics in human hepatocellular carcinoma. *Nano Res.* **2015**, *8*, 1729−1745.
11. John, J.V.; Seo, E.J.; Augustine, R.; Jang, I.H.; Kim, D.K.; Kwon, Y.W.; Kim, J.H.; Kim, I. Phospholipid end-capped bioreducible polyurea micelles as a potential platform for intracellular drug delivery of doxorubicin in tumor cells. *ACS Biomater. Sci. Eng.* **2016**, *2*, 1883−1893.
12. Zhang, Y.F.; Ying, H.Z.; Hart, K.R.; Wu, Y.X.; Hsu, A.J.; Coppola, A.M.; Kim, T.A.; Yang, K.; Sottos, N.R.; White, S.R.; Cheng, J.J. Malleable and recyclable poly(urea-urethane) thermosets bearing hindered urea bonds. *Adv. Mater.* **2016**, *28*, 7646−7651.
13. Jiang, Z.Y.; Chen, J.J.; Cui, L.G.; Zhuang, X.L.; Ding, J.X.; Chen, X.S. Advances in stimuli-responsive polypeptide nanogels. *Small Methods* **2018**, *2*, 307−321.
14. Tang, B.Q.; Zaro, J.L.; Shen, Y.; Chen, Q.; Yu, Y.L.; Sun, P.P.; Wang, Y.Q.; Shen, W.C.; Tu, J.S.; Sun, C.M. Acid-sensitive hybrid polymeric micelles containing a reversibly activatable cell-penetrating peptide for tumor-specific cytoplasm targeting. *J. Controlled Release* **2018**, *279*, 147−156.
15. Gao, S.T.; Tang, G.S.; Hua, D.W.; Xiong, R.H.; Han, J.Q.; Jiang, S.H.; Zhang, Q.L.; Huang, C.B. Stimuli-responsive bio-based polymeric systems and their applications. *J. Mater. Chem. B* **2019**, *7*, 709−729.
16. Shi, F.H.; Ding, J.X.; Xiao, C.S.; Zhuang, X.L.; He, C.L.; Chen, L.; Chen, X.S. Intracellular microenvironment responsive PEGylated polypeptide nanogels with ionizable cores for efficient doxorubicin loading and triggered release. *J. Mater. Chem.* **2012**, *22*, 14168−14179.
17. Chu, B.Y.; Qu, Y.; Huang, Y.X.; Zhang, L.; Chen, X.X.; Long, C.F.; He, Y.Q.; Ou, C.W.; Qian, Z.Y. PEG-derivatized octacosanol as micellar carrier for paclitaxel delivery. *Int. J. Pharm.* **2016**, *500*, 345−359.
18. Cheng, Y.L.; He, C.L.; Ding, J.X.; Xiao, C.S.; Zhuang, X.L.; Chen, X.S. Thermosensitive hydrogels based on polypeptides for localized and sustained delivery of anticancer drugs. *Biomaterials* **2013**, *34*, 10338−10347.
19. Zhang, Y.; Cai, L.L.; Li, D.; Lao, Y.H.; Liu, D.Z.; Li, M.Q.; Ding, J.X.; Chen, X.S. Tumor microenvironment-responsive hyaluronate-calcium carbonate hybrid nanoparticle enables effective chemotherapy for primary and advanced osteosarcomas. *Nano Res.* **2018**, *11*, 4806−4822.
20. Wang, Y.P.; Gao, W.Q.; Shi, X.Y.; Ding, J.J.; Liu, W.; He, H.B.; Wang, K.; Shao, F. Chemotherapy drugs induce pyroptosis through caspase-3 cleavage of a gasdermin. *Nature* **2017**, *547*, 99−103.
21. Chen, J.J.; Ding, J.X.; Wang, Y.C.; Cheng, J.J.; Ji, S.X.; Zhuang, X.L.; Chen, X.S. Sequentially responsive shell-stacked nanoparticles for deep penetration into solid tumors. *Adv. Mater.* **2017**, *29*, 170−177.
22. Han, J.D.; Zhao, X.Y.; Xu, W.G.; Wang, W.; Han, Y.P.; Feng, X.R. Effect of hydrophobic polypeptide length on performances of thermo-sensitive hydrogels. *Molecules* **2018**, *23*, 1017−1027.

23. Xu, W.G.; Ding, J.X.; Xiao, C.S.; Li, L.Y.; Zhuang, X.L.; Chen, X.S. Versatile preparation of intracellular-acidity-sensitive oxime-linked polysaccharide-doxorubicin conjugate for malignancy therapeutic. *Biomaterials* **2015**, *54*, 72–86.

24. Lv, Y.; Xu, C.; Zhao, X.; Lin, C.; Yang, X.; Xin, X.; Zhang, L.; Qn, C.; Han, X.; Yang, L.; He, W.; Yin, L. Nanoplatform assembled from a CD44-targeted prodrug and smart liposomes for dual targeting of tumor microenvironment and cancer cells. *ACS Nano* **2018**, *12*, 1519–1536.

Sample Availability: Samples of the compounds are available from the authors.